Bioelectrochemistry 141 (2021) 107870

Contents lists available at ScienceDirect

Bioelectrochemistry

journal homepage: www.elsevier.com/locate/bioelechem

Flexible electrochemical uric acid and glucose biosensor

Md Faruk Hossain, Gymama Slaughter *

Frank Reidy Research Center for Bioelectrics, Department of Electrical and Computer Engineering, Old Dominion University, Norfolk, VA 23528, USA

ARTICLE INFO

Article history:
Received 13 April 2021
Received in revised form 15 May 2021
Accepted 2 June 2021
Available online 6 June 2021

Keywords:
Laser scribed graphene
Platinum nanoparticles
Uric acid
Glucose
Flexible biosensors

ABSTRACT

Fully integrated uric acid (UA) and glucose biosensors were fabricated on polydimethylsiloxane/polyimide platform by facile one step laser scribed technique. The laser scribed graphene (LSG) on the thin polyimide film was functionalized using pyrenebutanoic acid, succinimide ester (PBSE) to improve the electrochemical activity of the biosensors. The LSG was further decorated with platinum nanoparticles (PtNPs) to promote the electrocatalytic activity towards the oxidation of UA. Glucose oxidase was immobilized on the PtNPs modified surface for selective detection of glucose. The fabricated biosensors were characterized via scanning electron microscopy (SEM), Energy dispersive X-ray (EDX), X-ray photoelectron spectroscopy (XPS), and electrochemical methods (cyclic voltammetry and amperometry measurements). Outstanding electrocatalytic activities toward oxidation of UA and glucose were demonstrated. A wide detection range of 5 μM to 480 μM UA with a high sensitivity of 156.56 μA/mMcm^2 and a calculated detection limit (LOD) of 0.018 μM (S/N = 3) were achieved for the UA biosensor. The glucose biosensor exhibited a detection range of 5 μM to 3200 μM with a sensitivity of 12.64 μA/mMcm^2 and an LOD of 2.57 μM (S/N = 3). These integrated biosensors offer great promise for potential applications in wearable UA and glucose sensing due to their good sensitivity, selectivity, and stability properties.

1. Introduction

Common metabolites (glucose, lactate, uric acid, etc.) and electrolytes (chlorine, sodium, etc.) are detected by wearable devices for non-intrusive, continuous, and noninvasive monitoring [1–4]. Uric acid (UA) has garnered attention as an endogenous biomarker for wound healing assessment [5,6]. In recent years, many efforts have demonstrated non-healing wounds have elevated levels of UA, where the UA can diffuse into the sweat glands and tissues present in the wound proximity [7,8]. Moreover, high glucose levels have been shown to weaken the bactericidal ability of white blood cells, thereby causing bacteria growth, slow healing, and infection at the wound site [9,10]. Individuals who experience poor wound healing associated with diabetes also encounter other complications, such as heart disease, kidney disease, and eye problems, etc. [11–15]. Although the detection of glucose is widely investigated [2,16–19], the assessment of both uric acid and glucose level are rare [20,21]. Flexible and stretchable platform can be realized through several complex clean room techniques including chemical vapor deposition, photolithography, dry etching, and film transfer [2,22–24]. Recently, laser scribed graphene (LSG) has attracted much attention due to its ease of fabrication and printing scalability on flexible and stretchable platform. LSG is a straightforward fabrication procedure, where CO_2 laser burns a polyimide film (PI) or Kapton tape to create a three-dimensional (3D) graphene pattern. In the patterned areas, sp^3-carbon atoms are transformed to sp^2-carbon atoms via the photothermal process. However, applying LSG in the fabrication of biosensors is challenging due to its poor mechanical stability, and electrical and chemical properties. Since LSG flakes can easily shed from the burnt surface, a few approaches have been proposed for modifying the LSG. To increase conductivity, Ye et al. prepared an LSG film with metal doping of the PI precursor [25]. Another group improved electrochemical properties by doping the PI film with boron [26]. To increase mechanical stability and conductivity, Zahed et al. sprayed coated PEDOT: PSS on the fabricated LSG [27]. To increase mechanical stability and conductivity, Park et al. sprayed coated PEDOT: PSS on the fabricated LSG [28]. Yoon et al. modified LSG using acetic acid solution to introduce oxygen functional groups in the LSG film leading to improved electrochemical activity [19]. Functional groups have been demonstrated to improve the anchoring sites for the decoration of nanoparticles and immobilization of enzyme [28,29]. The functionalization of LSG further enhances the interaction between LSG and loading materials, which modulates the tethering of nanomaterials and biomolecules. Due to the outstanding chemical properties of carboxylic groups-containing materials, COOH-substituted LSG is expected to have enhanced

* Corresponding author.
E-mail address: gslaught@odu.edu (G. Slaughter).

https://doi.org/10.1016/j.bioelechem.2021.107870
1567-5394/

functionalization efficiency compared to a pristine LSG and exhibit a promising tendency to bind nanomaterials and biological materials without perturbing original structure of carbon-based materials [30,31].

In this study, a fully integrated biosensor system was fabricated on polyimide platform via a one-step laser scribed technique. LSG flakes can easily detach from the substrate surface upon shedding and frequent bending, the shedding may further decrease the electrochemical properties of the LSG based biosensor. Here, the formed 3D graphene was functionalized using pyrenebutanoic acid, succinimide ester (PBSE) crosslinker to hold the LSG flakes intact on the PI surface and prevent the shedding of the LSG flakes and to improve the electrochemical activity of the LSG film. Since UA can easily be oxidized at common nonenzymatic biosensor, the LSG film was decorated with platinum nanoparticles (PtNPs) due to its outstanding catalytic activity towards biomolecules [32,33]. The biosensor based on LSG/PBSE/PtNPs exhibited a wide range concentration with good sensitivity. Additionally, the nanostructured surface provides a suitable microenvironment for enzyme immobilization and facilitates direct electron transfer between the active site of the enzyme and the electrode [34]. The as-fabricated functionalized LSG and anchored PtNPs modified biosensor offered an improved electrochemical activity and a good platform for enzyme immobilization. PtNPs serve as an inexpensive alternative to uricase enzyme for the determination of UA. To the best of our knowledge, this is the first report of a novel LSG functionalization with PBSE strategy to achieve electrochemically stable platform capable of detecting both uric acid and glucose biomarkers. The physicochemical analyses of the fabricated biosensors were conducted using field emission scanning electron microscopy (FESEM), energy dispersive X-ray spectroscopy (EDX), X-ray photoelectron spectroscopy (XPS), and electrochemical techniques.

2. Materials and methods

2.1. Chemicals

Potassium tetrachloroplatinate (K_2PtCl_4), sulphuric acid (H_2SO_4), uric acid (UA), glucose, glucose oxidase (GOx), (1-ethyl-3-(3-dimethylamino) propyl carbodiimide, hydrochloride (EDC), N-hydroxysuccinimide (NHS), ascorbic acid, sodium chloride, acetaminophen, potassium chloride, nafion 5% in H_2O were purchased from Sigma Aldrich Co USA. 1-Pyrenebutanoic acid, succinimidyl ester (PBSE) was obtained from Anaspec Inc. Polydimethylsiloxane (PDMS) and Kapton tape or polyimide film (PI, thickness of 50 μm) were ordered from Amazon Marketplace. The purchased chemicals were used without further purification. All stock solutions were prepared using 0.1 M phosphate buffered solution (PBS), and all other solutions were prepared with milli-Q water (MQ, resistivity ≥ 18 MΩ-cm).

2.2. Design and fabrication of integrated LSG three-electrode system

A PDMS mixture solution (10:1 wt%) was prepared and casted on a 4-inch silicon (Si) wafter followed by soft baking at 80 °C for 20 min. Upon drying, PI tape (w = 15 mm) was attached to the surface of the PDMS film. Fig. 1 provides an illustration of the integrated LSG three-electrode sensor design completed using AutoCAD software (Autodesk, Inc.) and patterned by a programmable BOSS Laser machine (BOSS LS-1630) on PI (Fig. 1A) and PI taped PDMS coated 4-inch silicon wafer (Fig. 1B). Briefly, CO_2 pulsed laser (speed 250 mm/s, pass-1, layer- black, power max-25%, min power 25%) was applied to the PI film to generate the 3D graphene pattern. The nonenzymatic uric acid biosensor

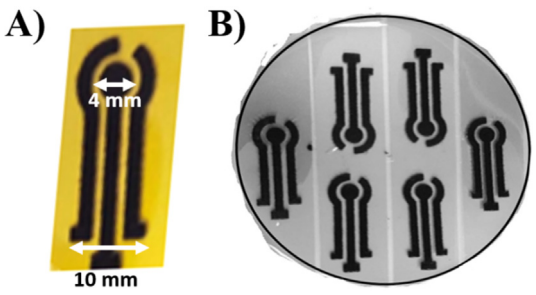

Fig. 1. Illustration of integrated three-electrode biosensor design on (A) polyimide (PI) and (B) PI taped polydimethylsiloxane (PDMS) coated on the 4-inch silicon wafer.

employs LSG/PBSE/PtNPs working electrode and the enzymatic glucose biosensor employs an LSG/PBSE/PtNPs/GOx/nafion working electrode. LSG/PBSE/PtNPs and Ag/AgCl paste were used as the counter and reference electrodes, respectively. The diameter of the working electrode is 4 mm with a pitch distance of 1.5 mm. The chemical and physical characteristics of the fabricated biosensors were investigated by high-resolution X-ray photoelectron spectroscopy (PHI VersaProbe III Scanning XPS) and scanning electron microscopy (Hitachi FE-SEM Su-70). Electrochemical deposition of PtNPs, amperometry, and cyclic voltammetry (CV) were performed via BASi Epsilon EClipse electrochemical workstation.

2.3. Modification of uric acid biosensor

30 mM PBSE was prepared in dimethyl sulfoxide (DMSO) and vigorously mixed using a vortex mixer. 10 μL of the prepared PBSE solution was carefully drop casted on the working and counter electrodes and allowed to dry in the dark overnight. The PBSE functionalized electrodes were rinse with DMSO followed by PBS rinse to remove any unbound PBSE and DMSO, respectively and provide carboxylic functional groups on the surface of the electrodes (Fig. 2). The electrochemical deposition of PtNPs on the working and counter electrodes was performed using a three-electrode configuration system via cyclic voltammetry with a potential window of − 0.2 V to 0.75 V in a precursor solution consisting of 2 mM of K_2PtCl_4 and 60 mM H_2SO_4 for 12 cycles and 20 cycles, respectively. The electrodes were then rinsed with Milli-Q water and used as the non-enzymatic LSG/PBSE/PtNPs UA biosensor. To realize the glucose biosensor, glucose oxidase (GOx) was immobilized on a separate LSG/PBSE/PtNPs working electrode. The carboxylic functional groups on the LSG/PBSE/PtNPs were activated via EDC/NHS coupling using 6.5 μL equimolar of EDC/NHS (20 mM) drop casted on the top of the modified working electrode. After 3 h of incubation at room temperature, 12.5 μL of GOx enzyme solution prepared from 2.5 mg/mL of GOx completely dissolved in a 1.25 mg/mL of chitosan–gelatin deionized water mixture was drop casted on the EDC/NHS treated surface. The biosensor immobilized with GOx was dried at 4 °C. A final 6.5 μL of nafion in ethanol/deionized water solution (1:7:1) was applied to the surface of the working electrode and dried at room temperature for 15 min. The glucose biosensor was stored at 4 °C for 24 h prior to use.

3. Results and discussion

3.1. Surface morphology and crystal structure characterization of the fabricated electrodes

The surface morphology of the fabricated electrodes was investigated using FESEM. The FESEM micrographs of the LSG and the

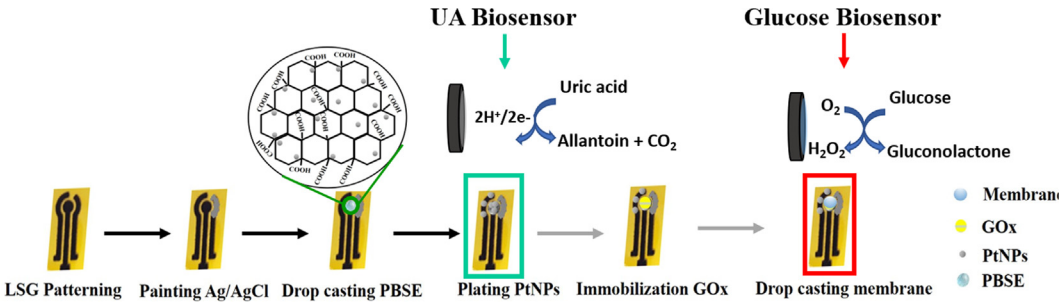

Fig. 2. Fabrication sequences of uric acid (UA) and glucose biosensors.

various surface modification are shown in Fig. 3. Fig. 3A shows the flaky uniform structure observed after laser scribing of the polyimide film. This flaked or wrinkled surface structure is typically expected after surface modification with graphene-based materials. Upon surface functionalization with PBSE, a network structure is observed on the LSG surface (Fig. 3B), thereby indicating that the aromatic and reactive ester groups attached to the surface of the LSG by π- π interaction [35]. The interpenetrating networks between LSG and PBSE is shown to improve the electrochemical activity (Fig. 4). PtNPs can be observed dispersed on the walls of the network structure of LSG/PBSE in Fig. 3C (Insert: Closeup view) upon electrodeposition. The PtNPs were on average 95 ± 8 nm in diameter and formed conductive pathways to enable electron transfer for both non-enzymatic and enzymatic biosensing with large surface area to enable efficient oxidation of UA molecules and immobilization of GOx. Furthermore, the decorated surface creates a favorable microenvironment for enzyme immobilization. GOx was subsequently immobilized on the PtNPs modified surface followed by nafion coating as shown in Fig. 3D. The enzyme and nafion tightly bound to the surface of the electrode and resulted in a smoother morphology for the sensing layer.

The elemental compositions of the LSG/PBSE/PtNPs electrode were investigated via EDX to confirm the electrodeposition of PtNPs. Fig. 3E shows the typical EDX pattern for the LSG/PBSE/PtNPs with a clear signal of the presence of C, O, and Pt. The weight percentages of C, O, and PtNPs were 85.23%, 10.2%, and 4.57%, respectively. This finding further indicates that the PtNPs were deposited on the LSG/PBSE modified surface. The chemical composition of LSG and the interaction between LSG and PBSE was

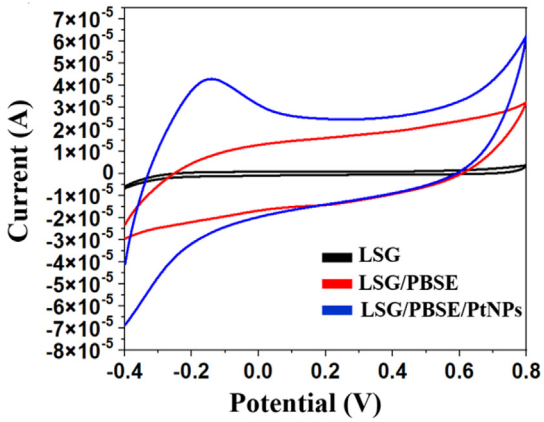

Fig. 4. Cyclic voltammogram (CV) of LSG, LSG/PBSE and LSG/PBSE/ PtNPs electrodes in 0.1 M PBS, pH 7, scan rate 50 mV/s.

evaluated using X-ray photoelectron spectroscopy (XPS) as illustrated in Fig. 3F. Both LSG and LSG/PBSE contain of C, O and Si elements and the presence of organic Si is attributed to the Si in the PDMS substrate material. No visible peak was observed for nitrogen and previous study noted that this may be due to the depth burning of polyimide and elimination of nitrogen from the surface of the substrate [36]. After functionalizing the LSG surface with PBSE, the oxygen content increased, whereas the carbon content decreased indicating successful conjugation of PBSE to LSG. In the deconvoluted C 1s spectra for the LSG (Fig. 3G), four different

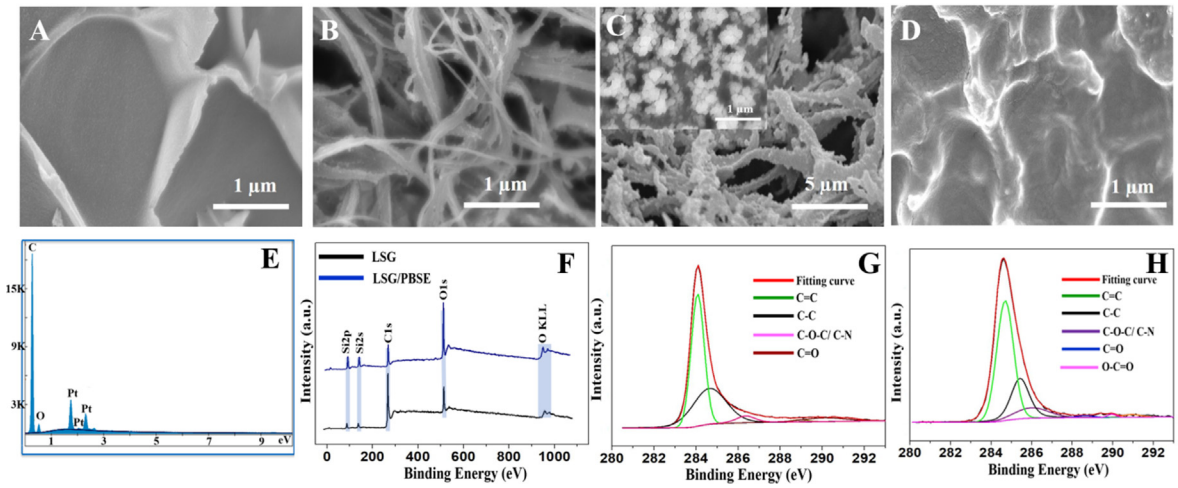

Fig. 3. Scanning electron microsopy (SEM) micrograph of (A) LSG, (B) LSG/PBSE, (C) LSG/PBSE/PtNPs, (D) LSG/PBSE/PtNPs/GOx /nafion modified electrodes, (E) Energy dispersive X-ray (EDX) analysis of LSG/PBSE/PtNPs, (F) X-ray photoelectron spectroscopy (XPS) survey spectra of LSG and LSG/PBSE, (G) XPS spectra of (G) LSG and (H) LSG/PBSE.

carbon states were observed as reported XPS for reduced graphene oxide (RGO) composite material [37]. The peaks centered at binding energies of 284.1 eV, 284.72 eV, 286.4 eV, and 290.15 eV. The two strong signals in the pristine LSG refer to the non-oxygenated ring C included in C=C to form sp2 hybridized carbon (green) and the sp3 hybridized carbon and includes the C-C (black). The broad band further deconvoluted into C–O–C/C-N at 286.4 eV (pink) that correspond to ether or amine groups, and O-C=O at 290.15 eV (brown) and is associated with carboxylic groups. Five peaks were observed in the LSG/PBSE XPS spectra (Fig. 3H) at binding energies 284.7 eV, 285.4 eV, 286.05 eV, 288.6 eV and 290.05 eV. Although the functional groups of LSG and LSG/PBSE are almost identical, two new peaks for PBSE conjugated LSG at 288.6 eV and 290.05 eV were observed to be associated with carbonyl and ester groups, respectively.

3.2. Electrochemical characterization of LSG/PBSE/PtNPs

Cyclic voltammetry (CV) was performed to investigate the electrocatalytic activity of LSG and modified electrode surfaces. Fig. 4 shows the CV voltammogram of LSG, LSG/PBSE, and LSG/PBSE/PtNPs electrodes in 0.1 M PBS solution Fig. 4. The bare LSG electrode exhibited the smallest current response, whereas the PBSE modified LSG electrode displayed a significant current response. The LSG/PBSE/PtNPs shows an enhanced catalytic current response with a characteristic peak at ca. −0.2 V for PtNPs in PBS. The electroactive surface area of the bare LSG and the modified LSG electrodes were calculated using Randles-Sevcik equation in 5 mM $K_3Fe(CN)_6$ as the redox probe [36]:

$$I_p = 2.65 \times 10^5 A D^{1/2} n^{3/2} v^{1/2} C \quad (1)$$

where n is the number of electrons (n = 1), A is the effective electroactive surface area (cm^2), D is the diffusion coefficient of the redox probe (6.70×10^6 cm^2 s^{-1}), C is the concentration of the electrolyte solution, υ is the scan rate (V s^{-1}), and I_p is the peak oxidation current (mA). The calculated electroactive surface area of the LSG and LSG/PBSE are 12.65×10^{-3} cm^2 and $7.58 \times 10^{-2} cm^2$, respectively. After the electrodeposition PtNPs, the electroactive surface area was calculated to be 1.1 $x10^{-1}$ cm^2, thereby resulting in an increased in the electroactive surface area of the electrode.

3.3. Electrochemical performance of LSG/PBSE/PtNPs towards the oxidation of UA

The electrochemical performance of the LSG-PBSE/PtNPs was investigated in 0.1 M PBS, pH 7. Fig. 5A shows the CV in the presence of successive uric acid injection in PBS. A well-defined oxidation peak for the uric acid was observed between 0.35 V and 0.40 V, wherein the anodic current increased with increasing uric acid concentration up to 250 μM. The first anodic peak observed in the voltammogram at −0.2 V is attributed to the presence of PtNPs in aqueous solution, where oxygen absorbs on the surface of PtNPs and is subsequently catalyzed to generate hydroxyl radicals via interaction with H_2O. The second peak at 0.35 V is attributed to the oxidation of uric acid in the presence of catalytic PtNPs. The oxidizing hydroxyl radicals generated on the surface of PtNPs oxidize the uric acid to produce allantoin, two electrons and two protons with CO_2 as the byproduct (see Fig. 2) at a potential between 0.3 V and 0.4 V [38]. Although the oxidation peak at −0.2 V increased in the presence of uric acid, it quickly saturated whereas the peak at 0.35 V linearly increased up to 250 μM uric acid. The corresponding calibration curves of the oxidation currents obtained at 0.35 V and 0.40 V exhibited a sensitivity of 25.28 μA/mM cm^2 and 26.24 μA/mM cm^2, respectively. Amperometric characterization of the UA biosensor was carried out at the lower potential of 0.35 V to reduce the interference effects of electroactive species. The nanostructured morphology of PtNPs provides a large surface area with numerous catalytic sites for the catalytic oxidation of uric acid molecules [32].

Fig. 5B demonstrates the electrocatalytic process of uric acid (100 μM) at different scan rate (20 mV/s – 120 mV/s). The corresponding anodic and cathodic calibration curves are shown in Fig. 5C. The anodic and cathodic peak currents exhibit good linear relationship with the square root of scan rate with a linear correlation coefficient of 0.997 and of 0.996 for the anodic and cathodic currents, respectively. The fabricated LSG/PBSE/PtNPs exhibited a diffusion-controlled process. Fig. 5D shows the amperometric responses of the LSG, LSG/PBSE, and LSG/PBSE/PtNPs electrodes in the presence of increasing concentration of uric acid. The experimental results shows that the LSG/PBSE/PtNPs electrode demonstrated the highest current response and sensitivity to uric acid compared to the bare LSG and LSG/PBSE electrodes. The oxidation of uric acid occurred rapidly in the presence of PBSE anchored PtNPs on LSG (Fig. 5D), indicating that anchored PtNPs exhibited very good catalytic activity toward uric acid. In addition, the LSG/PBSE/PtNPs nanocomposite provides high edge density per unit normal area compared to LSG nanostructures, thereby leading to fast electron transfer process which improve the electroactive activity, sensitivity, and overall performance of the electrochemical detection of uric acid. The LSG electrode showed no evident catalytic activity towards the oxidation of uric acid. In contrast, PtNPs synthesized according to the method reported by Hossain et al. and Kaur et al, showed lower sensitivity towards the oxidation of uric acid under the same conditions [32,39]. This further confirm the improved electrochemical performances of LSG/PBSE/PtNPs uric acid biosensor.

Fig. 5E provides the amperometric response of the LSG/PBSE/PtNPs upon successive injection of different concentration of uric acid at an applied potential of 0.35 V and corresponding calibration curve is depicted in Fig. 5E. The current increased instantly with each addition of uric acid aliquot and rapidly reached 95% steady state with a fast response time of 5 s. A linear detection range of 5 μM to 480 μM uric acid with a sensitivity of 156.56 μA/mM cm^2 (r^2 = 0.997) were observed. This linear range covers the normal range of UA level (155 μM to 428 μM) in serum and elevated levels of UA have been demonstrated to correlate with disease [7–10,40]. The calculated limit of detection of the fabricated biosensor was determined to be 0.18 μM (S/N = 3), which is well below the normal UA level. The performance of the uric acid biosensor was compared to other recent reports as shown in Table 1. The enhanced sensitivity of the nonenzymatic LSG/PBSE/PtNPs UA biosensor is higher than those reported for non-enzymatic PtNPs based UA biosensors [32,39], graphene-PtNPs UA biosensors [41], enzyme-based biosensor, and bare graphene UA biosensors [8,21]. The enhanced sensitivity can be ascribed to the large surface area and the synergistic effect of PtNPs on the electrocatalytic activity towards uric acid.

3.4. Electrochemical performance of LSG/PBSE/PtNPs/GOx/Nafion

The enzymatic glucose biosensor was prepared using GOx enzyme tethered to the PtNPs modified working electrode. Fig. 6A shows the CV of the glucose biosensor in the presence (red curve) and absence of glucose (black curve – PBS only). In the presence of 0.3 mM glucose, the biosensor exhibited an oxidation peak at ca. 0.5 V. The amperometric measurements were carried out at the onset (0.4 V) and peak oxidation potentials (0.5 V and 0.55 V) in 0.1 M PBS upon successive addition of different concentrations of glucose (Fig. 6B). The highest sensitivity of 12.64 μA/mMcm^2 was achieved with an applied potential of 0.5 V. Fig. 6C shows the amperometric response of the biosensor in PBS solution

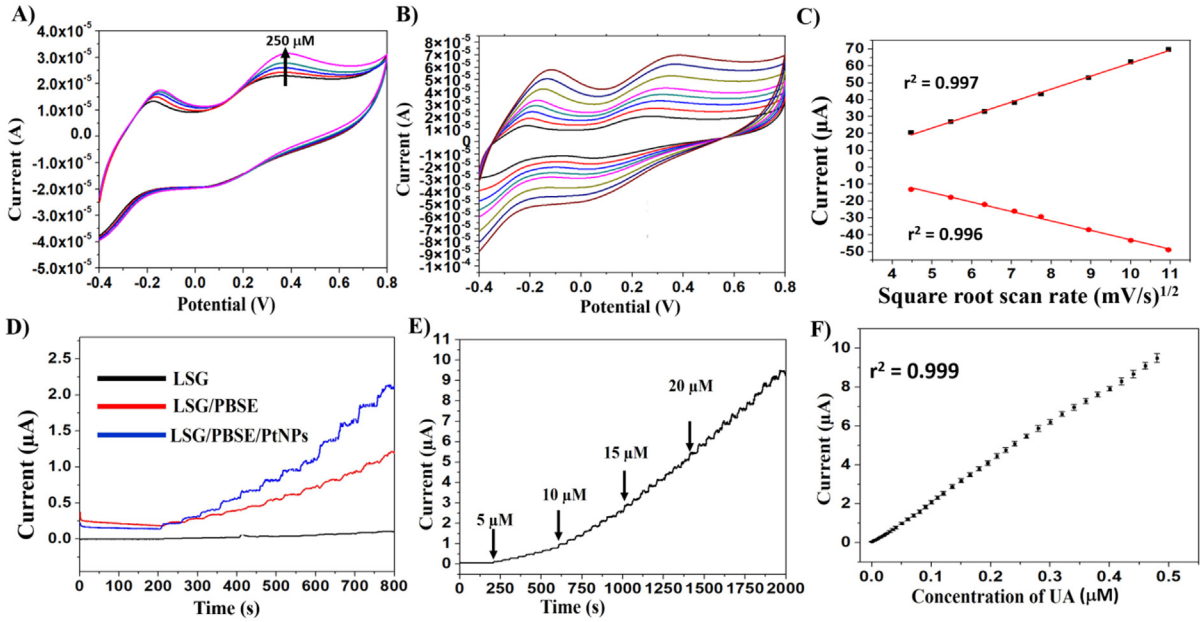

Fig. 5. CV of LSG-PBSE/PtNPs in PBS at (A) different concentrations of uric acid (0–250 μM), scan rate 50 mV/s, (B) 100 μM uric acid at different scan rates (20 mV/s – 120 mV/s), (C) Linear plot of anodic and cathodic peak currents, (D) Current-time curves of different LSG and LSG modified electrodes in 0.1 M PBS, pH 7 to different concentration of UA at 0.35 V, (E) Amperometric responses of LSG-PBSE/PtNPs in PBS to the successive injection of different concentration of UA at 0.35 V, and (F) Corresponding calibration curve with error bar (triplicates).

Table 1
Comparison of different uric acids sensors.

Electrode material	Response time (s)	LOD (μM)	Detection techniques	Linear range (mM)	Sensitivity (μA/mM cm^2)	Ref
Au/CG/PDDA/PtNPs	5	0.25	Amperometric	0.001–6.2	88.11	[32]
CNT/Au/HRP /UOx	–	9.91	CV	50–650	35.71	[8]
LEG-CS		0.74	DPV	–	3.50	[21]
GCE/RGO/PtNPs	–	0.45	DPV	10–130	–	[39]
PtNPs/ RG	–	0.22	DPV	0.0005–0.180	–	[41]
LSG/PBSE/PtNPs	5	0.18	Amperometric	0.005–0.480	156.56	This work

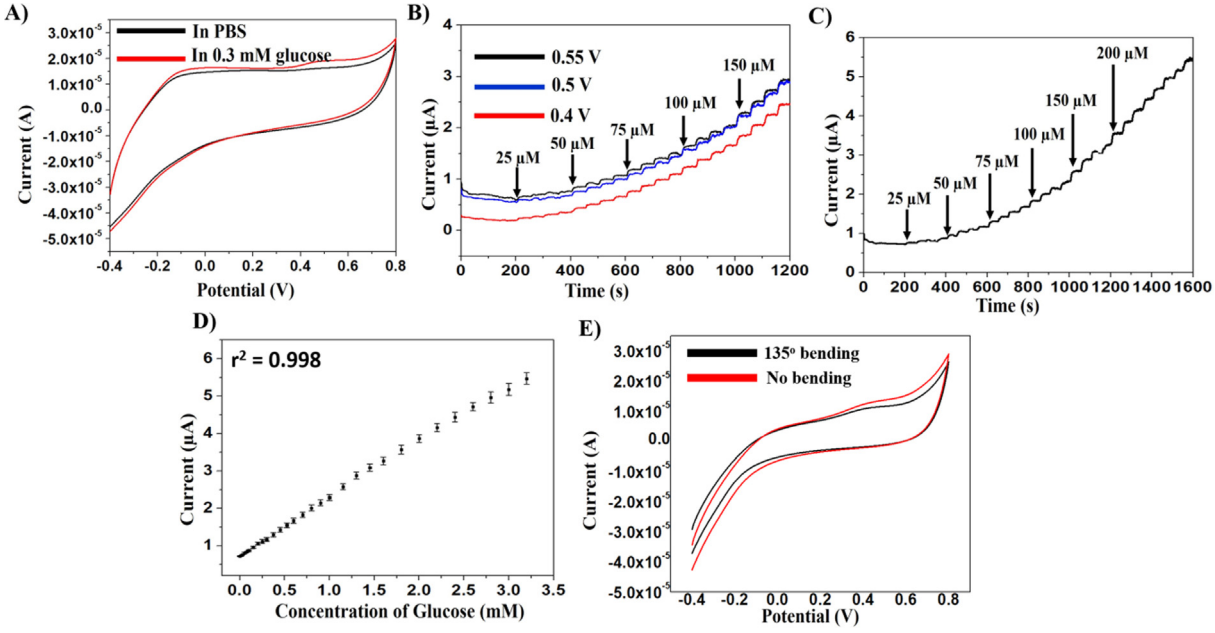

Fig. 6. (A) CV of glucose biosensor in with PBS and 0.3 mM glucose solution, scan rate 50 mV/s, (B) Current-time curves of the fabricated glucose sensor in 0.1 M PBS, pH 7 with different concentration of glucose at different potentials, (C) Amperometric current responses of glucose sensor in 0.1 M PBS to the successive addition of different concentration of glucose at 0.35 V, (D) Corresponding calibration curve with error bar (triplicates) and (E) CV of the LSG/PBSE/PtNPs before and after bending at 135° bend angle.

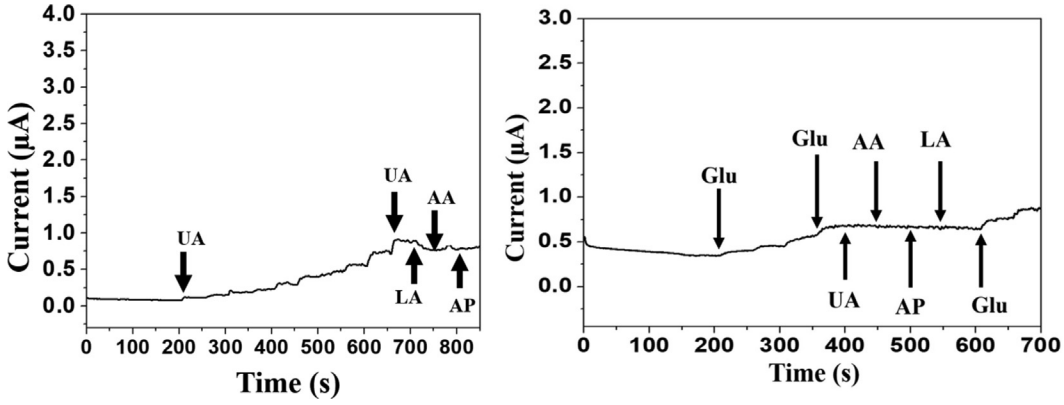

Fig. 7. Amperometric response of (A) UA and B) glucose biosensor to interfering analyte.

Table 2
Comparison of different glucose sensors.

Electrode matrix	Responsetime (s)	LOD (μM)	Potential (V)	Linear range (mM)	Sensitivity (μA/mM cm^2)	Ref
PET/Au/PB/CS/GOx	5	–	0	0.0–0.2	2.35	[2]
PDMS/Ti/Au/PB/GOx	–	9.91	–	0.06–1	26.31	[42]
Porous Au/PB/GOx/nafion		<10	–	0.01–1	3.50	[16]
LSG/PBSE/PtNPs/Gox/nafion	6	2.35	0.5	0.0025–2.5	12.64	This work

upon successive addition of different concentration of glucose at 0.5 V with the corresponding calibration curve shown in Fig. 6D. The biosensor responded very quickly and reach steady state within 6 s. A linear dynamic range of 25 μM to 3.2 mM with a linear correlation coefficient of 0.998 and a calculated limit of detection of 2.57 μM glucose was observed to cover the hypoglycemic range. Our fabricated glucose biosensor demonstrates an extended linear dynamic range and LOD than previously reported glucose biosensors [2,16,42]. The deformation of the flexible LSG/PBSE/PtNPs/GOx/Nafion when bent at 135° was examined in 0.3 mM glucose via cyclic voltammetry. Although no detrimental signal was observed in the voltammograms after bending, the oxidation current decreased after bending (black curve). This indicates that the electrode can generate adequate electrochemical signal while tolerating up to 135° bend angle. Table 2 provides the comparative performance of the fabricated glucose biosensor to reported flexible glucose biosensors.

3.5. Anti-interference and stability of biosensor

Fig. 7A and 7B show the amperometric responses of the UA and glucose biosensors, respectively. In the presence of 32 μM UA and common interfering species, ascorbic acid (0.1 mM AA), lactic acid (3 mM LA) and acetaminophen (0.1 mM AP), the UA biosensor exhibited good selectivity towards UA sensing, wherein insignificant current responses were observed in the presence of AA and AP at an applied potential of 0.35 V. However, the addition of 3 mM LA resulted in a reduction current that impacted the selectivity of the as-fabricated UA biosensor. To investigate the selectivity of the glucose biosensor, all the four interfering species exhibited little or no significant impact on the amperometric current response at the applied potential of 0.5 V. These results indicate that the fabricated biosensors are selective towards UA and glucose. Five identically fabricated UA and glucose biosensors were exposed to successive addition of 2 μM UA and 0.2 mM glucose in triplicates, respectively. Relative standard deviation (RSD) of 5.4% and 4.8% were observed in the amperometric responses for UA and glucose, respectively. Thereby indicating acceptable reproducibility of the fabricated biosensors. The stability of the biosensors was also investigated for a period of 7 weeks by monitoring the peak oxidation current response in the presence of the target analyte. 6.5% and 5.7% decreased in the sensitivities of the UA and glucose biosensors were observed over that period, respectively. Thereby indicating good stability for the biosensors.

4. Conclusions

UA and glucose biosensors have been successfully fabricated on flexible polyimide thin film laminated PDMS substrate. The fabricated biosensors exhibited excellent catalytic activity towards oxidation of UA over a wide linear range of 5 μM to 480 μM with a sensitivity of 156.56 μA/mMcm^2 UA. After immobilization of GOx on the PtNPs modified working electrode, a glucose biosensor was realized. The fabricated glucose biosensor exhibited good electrocatalytic activity towards oxidation of glucose with a sensitivity of 12.74 μA/mMcm^2 and a wide linear range of 5 μM to 3200 μM. The biosensors demonstrated good anti-interference ability and stability for detection of the target analytes. These results demonstrate that PtNPs integrated on LSG provides a high surface area with good electrocatalytic activity towards UA and when coupled with glucose specific enzyme serves as a good biosensing platform.

Declaration of Competing Interest

The author declare that there is no conflict of interest.

Acknowledgments

Research supported by United States Army Medical Research and Materials Command (USAMRMC W81XWH-17-1-0452).

References

[1] A.J. Bandodkar, W. Jia, C. Yardimci, X. Wang, J. Ramirez, J. Wang, Tattoo-based noninvasive glucose monitoring: a proof-of-concept study, Anal. Chem. 87 (2015) 394–398.
[2] W. Gao, S. Emaminejad, H.Y. Nyein, S. Challa, K. Chen, A. Peck, H.M. Fahad, H. Ota, H. Shiraki, D. Kiriya, D.-H. Lien, G.A. Brooks, R.W. Davis, A. Jave, Fully

integrated wearable sensor arrays for multiplexed in situ perspiration analysis, Nature 529 (2016) 509–514.
[3] G. Slaughter. Current Advances in biosensor design and fabrication., Encyclopedia of Analytical Chemistry: Applications, Theory and Instrumentation, (2006), 1-25.
[4] J.S. Narayanan, G. Slaughter, AuNPs-HRP microneedle biosensor for ultrasensitive detection of hydrogen peroxide for organ preservation, Medical Devices & Sensors 1 (2018) e10015.
[5] M.L. Fernandez, Z. Upton, H. Edwards, K. Finlayson, G.K. Shooter, Elevated uric acid correlates with wound severity, Int. Wound J. 9 (2012) 139–149.
[6] P. Kassal, J. Kim, R. Kumar, W.R. de Araujo, I.M. Steinberg, M.D. Steinberg, J. Wang, Smart bandage with wireless connectivity for uric acid biosensing as an indicator of wound status, Electrochem. Commun. 56 (2015) 6–10.
[7] J.M. McCord, Oxygen-derived free radicals in postischemic tissue injury, New England J. Med. 312 (1985) 159–163.
[8] P. Bhushan, Y. Umasankar, S.R. Choudhury, P.A. Hirt, F.E. MacQuhaec, L.J. Borda, H.A. Lev-Tov, R.S. Kirsner, S. Bhansali, Biosensor for monitoring uric acid in wound and its proximity: a potential wound diagnostic tool, J. Electrochem. Soc. 166 (2019) B830–B836.
[9] J. Zhu, G. Jiang, W. Hong, Y. Zhang, B. Xu, G. Song, T. Liua, C. Honga, L. Ruan, Rapid gelation of oxidized hyaluronic acid and succinyl chitosan for integration with insulin-loaded micelles and epidermal growth factor on diabetic wound healing, Material. Sci. Eng. C 117 (2020) 111273.
[10] K. Miyajima, S.H. Teoh, H. Yamashiro, M. Shinohara, F. Fatchiyah, T. Ohta, T. Yamada, Effects on glycemic control in impaired wound healing in spontaneously diabetic torii (SDT) fatty rats, Med Arch. 72 (2018) 4–8.
[11] D.G. Greenhalgh, Wound healing and diabetes mellitus, Clin Plastic Surg 30 (2003) 37–45.
[12] U.A. Okonkwo, L.A. DiPietro, Diabetes and wound angiogenesis, Int. J. Mol. Sci. 18 (2017) 1419.
[13] A. Dehghan, M. van Hoek, E.J.G. Sijbrands, A. Hofman, J.C.M. Witteman, High serum uric acid as a novel risk factor for type 2 diabetes, Diabetes Care 31 (2008) 361–362.
[14] I. Hameed, S.R. Masoodi, S.A. Mir, M. Nabi, K. Ghazanfar, B.A. Ganai, Type 2 diabetes mellitus: from a metabolic disorder to an inflammatory condition, World J. Diabetes 6 (2015) 598–612.
[15] P. Saeedi, I. Petersohn, P. Salpea, B. Malanda, S. Karuranga, N. Unwin, S. Colagiuri, L. Guariguata, A. A. Motala, K. Ogurtsova, J.E. Shaw, D. Bright, R. Williams, On behalf of the IDF Diabetes Atlas Committee, Global and regional diabetes prevalence estimates for 2019 and projections for 2030 and 2045: Results from the International Diabetes Federation Diabetes Atlas, 9th edition, Diabetes research and clinical practice 157 (2019) 107843.
[16] Y. Zhang, N. Li, Y. Xiang, D. Wang, P. Zhang, Y. Wang, S. Lu, R. Xu, J. Zhao, A flexible non-enzymatic glucose sensor based on copper nanoparticles anchored on laser-induced graphene, Carbon 156 (2020) 506–513.
[17] J.D. Yuen, A. Baingane, Q. Hasan, L.C. Shriver-Lake, S.A. Walper, D. Zabetakis, J. C. Breger, D.A. Stenger, G. Slaughter, A fully-flexible solution-processed autonomous glucose indicator, Sci. Rep. 9 (2019) 1–9.
[18] J.S. Narayanan, G. Slaughter, Towards a dual in-line electrochemical biosensor for the determination of glucose and hydrogen peroxide, Bioelectrochemistry 128 (2019) 56–65.
[19] H.S. Yoon, J.S. Nah, H. Kim, S. Ko, M. Sharifuzzaman, S.C. Barman, X. Xuan, J. Kim, J.Y. Park A chemically modified laser-induced porous graphene based flexible and ultrasensitive electrochemical biosensor for sweat glucose detection, Sensor. Actuator. B Chem. 311 (2020) 127866.
[20] N. Liappis, S.D. Kelderbacher, K. Kesseler, P. Bantzer, Quantitative study of free amino acids in human eccrine sweat excreted from the forearms of healthy trained and untrained men during exercise, Eur. J. Appl. Physiol. Occup. Physiol. 42 (1979) 227–234.
[21] Y. Yang, Y. Song, X. Bo, J. Min, O.S. Pak, L. Zhu, M. Wang, J. Tu, A. Kogan, H. Zhang, T.K. Hsiai, Z. Li, Wei Gao, A laser-engraved wearable sensor for sensitive detection of uric acid and tyrosine in sweat, Nat. Biotech. 38 (2020) 217–224.
[22] R.K. Pal, S. Pradhan, L. Narayanan, V.K. Yadavalli, Micropatterned conductive polymer biosensors on flexible PDMS films, Sens. Actuat., B 259 (2018) 498–504.
[23] R. Li, H. Qi, Y. Ma, Y. Deng, S. Liu, Y. Jie, J. Jing, J. He, X. Zhang, L. Wheatley, C. Huang, X. Sheng, M. Zhang, L. Yin, A flexible and physically transient electrochemical sensor for real-time wireless nitric oxide monitoring, Nat. Commun. 11 (2020) 3207.
[24] S. Imani, A.J. Bandodkar, A.M.V. Mohan, R. Kumar, S. Yu, J. Wang, Patrick P. Mercier, A wearable chemical–electrophysiological hybrid biosensing system for real-time health and fitness monitoring, Nat. Commun. 7 (2016) 11650.
[25] R. Ye, Z. Peng, T. Wang, Y. Xu, J. Zhang, Y. Li, L.G. Nilewski, J. Lin, J.M. Tour, Situ formation of metal oxide nanocrystals embedded in laser-induced graphene, ACS Nano 9 (2015) 9244.
[26] Z. Peng, R. Ye, J.A. Mann, D. Zakhidov, Y. Li, P.R. Smalley, J. Lin, J.M. Tour, Flexible Boron-doped laser-induced graphene microsupercapacitors, ACS Nano 9 (2015) 5868–5875.
[27] M.A. Zahed, P.S. Das, P. Maharjan, S.C. Barman, M. Sharifuzzaman, S.H. Yoon, J. Y. Park, Flexible and robust dry electrodes based on electroconductive polymer spray-coated 3D porous graphene for long-term electrocardiogram signal monitoring system, Carbon 165 (2020) 26–36.
[28] M. Zhu, Y. Dong, B. Xiao, Y. Du, P. Yang, X. Wang, Enhanced photocatalytic hydrogen evolution performance based on Ru-trisdicarboxybipyridine-reduced graphene oxide hybrid, J. Mater. Chem. 22 (2012) 23773–23779.
[29] M.F. Hossain, G. Slaughter, PtNPs decorated chemically derived graphene and carbon nanotubes for sensitive and selective glucose biosensing, J. Electroanal. Chem. 861 (2020) 113990.
[30] M. Bourourou, K. Elouarzaki, N. Lalaoui, C. Agnes, A.L. Goff, M. Holzinger, A. Maaref, S. Cosnier, Supramolecular immobilization of laccase on carbon nanotube electrodes functionalized with (methylpyrenylaminomethyl) anthraquinone for direct electron reduction of oxygen, Chem.–Eur. J. 19 (2013) 9371–9375.
[31] A. Navaeea, A. Salimi, Graphene-supported pyrene-functionalizedamino-carbon nanotube: a novel hybrid architecture of laccase immobilization as effective bioelectrocatalyst for oxygen reduction reaction, J. Mater. Chem. A 3 (2015) 7623–7630.
[32] M.F. Hossain, S.C. Barman, J.Y. Park, Seed-mediated growth of platinum nanoparticles anchored on chemically modified graphene and cationic polyelectrolyte composites for electrochemical multi-sensing applications, Sens. Actuat., B 282 (2019) 780–789.
[33] S. Hrapovic, Y. Liu, K.B. Male, J.H.T. Luong, Electrochemical biosensing platforms using platinum nanoparticles and carbon nanotubes, Anal. Chem. 76 (2004) 1083–1088.
[34] X. Chen, G. Wu, Z. Cai, M. Oyama, X. Chen, Advances in enzyme-free electrochemical sensors for hydrogen peroxide, glucose, and uric acid, Microchim Acta 181 (2014) 689–705.
[35] L. Guadagno, M. Raimondo, L. Vertuccio, C. Naddeo, G. Barra, P. Longo, P. Lamberti, G. Spinelli, M.R. Nobile, Morphological, rheological and electrical properties of composites filled with carbon nanotubes functionalized with 1-pyrenebutyric acid, Compos. B 147 (2018) 12–21.
[36] A. Lamberti1, F. Perrucci, M. Caprioli, M. Serrapede, M. Fontana, S. Bianco1, S. Ferrero, E. Tresso, New insights on laser-induced graphene electrodes for flexible supercapacitors: tunable morphology and physical properties, Nanotechnology 28 (2017) 174002.
[37] Y. Wang, X. Di, X. Gao, X. Wu, Design of MOF-derived hierarchical Co@ C@ RGO composite with controllable heterogeneous interfaces as a high-efficiency microwave absorbent, Nanotechnology 31 (2020) 395710.
[38] J.A. Hondred, I.L. Medintz, J.C. Claussen, Enhanced electrochemical biosensor and supercapacitor with 3D porous architectured graphene via salt impregnated inkjet maskless lithography, Nanoscale Horiz. 4 (2019) 735–746.
[39] B. Kaur, T. Pandiyan, B. Satpati, R. Srivastava, Simultaneous and sensitive determination of ascorbic acid, dopamine, uric acid, and tryptophan with silver nanoparticles-decorated reduced graphene oxide modified electrode, Colloids Surf. BBiointerfaces 111 (2013) 97–106.
[40] G. Desideri, G. Castaldo, A. Lombardi, M. Mussap, A. Testa, R. Pontremoli, L. Punzi, C. Borghi, Is it time to revise the normal range of serum uric acid levels, Eur Rev Med Pharmacol Sci 18 (2014) 1295–1306.
[41] Hui Zhou, Wenmin Wang, Ping Li, Yu. Yongfang, Lu. Limin, Sensitive electrochemical determination uric acid at Pt nanoparticles decorated graphene composites in the presence of dopamine and ascorbic acid, Int. J. Electrochem. Sci. 11 (2016) 5197–5206.
[42] T.Q. Xu, Q.L. Zhang, J.N. Zheng, Z.Y. Lv, J. Wei, A.J. Wang, J.J. Feng, Simultaneous determination of dopamine and uric acid in the presence of ascorbic acid using Pt nanoparticles supported on reduced graphene oxide, Electrochim. Acta 115 (2014) 109–111.